PCCP

Accepted Manuscript

ROYAL SOCIETY OF CHEMISTRY

www.rsc.org/pccp

Physical Chemistry Chemical Physics
CREATED USING THE RSC LaTeX PCCP ARTICLE TEMPLATE – SEE www.rsc.org/electronicfiles FOR DETAILS
ARTICLE TYPE www. rsc.org/xxxxxx | XXXXXXXX

Metal-Free Ferromagnetic Metal and Intrinsic Spin Semiconductor: Two Different Kind of SWCNT Functionalized BN Nanoribbons

Ping Lou

Received Xth XXXXXXXXXX 20XX, Accepted Xth XXXXXXXXX 20XX
First published on the web Xth XXXXXXXXXX 200X
DOI: 10.1039/b000000x

Two different kind of SWCNT functionalized zigzag edge BN nanoribbons with n chains (n-ZBNNRs), namely, (a) B-edge functionalized by (m,m)SWCNT and N-edge modified with H (nZBNNR-B-(m,m)SWCNTs), (b) the B-edge modified with H and the N-edge functionalized by (m,m)SWCNT (nZBNNR-N-(m,m)SWCNTs), have been predicted. Amazingly, we find that unlike the semiconducting and nonmagnetic H-modified n-ZBNNRs, the nZBNNR-B-(m,m)SWCNTs are the intrinsic ferromagnetic metals, regardless of ribbon widths n and tube diameters (m,m). At a given (m,m), its local magnetic moments, at first, exhibit oscillation with increasing n, whereas when n is larger than 5, they are independent of n. In contrast, unlike the metallic and nonmagnetic (m,m)SWCNTs, the nZBNNR-N-(m,m)SWCNTs are the ferromagnetic intrinsic spin-semiconductors with direct band gap, regardless of n and (m,m). Its local magnetic moments and band gaps are independent of n and (m,m). The DFT calculations reveal that the process of the SWCNT functionalized n-ZBNNRs does not need any activation energy. Moreover, the formation energies of the SWCNT functionalized n-ZBNNRs are always less than zero. Therefore, the SWCNT functionalized n-ZBNNRs not only are steady, but also can be spontaneously formed. Furthermore, compared with n-ZBNNRs, the SWCNT functionalized n-ZBNNRs show significant improvement in the thermal and mechanical stabilities. Thus, (m,m)SWCNT functionalization of n-ZBNNRs may open new routes toward practical nanoelectronic and optoelectronic as well as spintronic devices based on BNC-based materials.

1 Introduction

In the past few decades, graphene nanoribbons (made by cutting graphene or unzipping carbon nanotubes) and single-walled carbon nanotubes (SWCNTs, one dimensional hollow cylindrical nanostructures) have wined considerable attention owing to their unique and fascinating properties,[1–34] One of the most striking characteristics of graphene nanoribbons is the sensibility of its properties to the details of the edge shape, such as, H-passivated armchair edge graphene nanoribbons possess nonmagnetic semiconducting ground states, while H-passivated zigzag edge graphene nanoribbons possess magnetic semiconducting ground states which each zigzag edge posses ferromagnetic order, but between the edge magnetic coupling are antiferromagnetic coupling.[1] Such edge magnetisms originate from its peculiar edge state[2–4] and provide a new model for potential applications in spintronics.[5–7] Whereas, if the edges are not straight, the edge magnetic coupling can be different, such as a ferromagnetic coupling, instead of usual antiferromagnetic coupling.[8,9] In addition, due to the chemical activity of the graphene nanoribbon edges,[10–12] its electronic and magnetic properties can be modified by the termination and passivation of edges.[13–17] Recently, Tang et al. have studied semiconductor-half-metal transition in zigzag graphene nanoribbons supported on hybrid fluorographene-graphane nanoribbons.[18] On the other hand, SWCNTs can be considered to be rolled from graphene,[19–22] and thus, the geometric structure of a SWCNT can be described by its chiral indices (m,l) that define its perimeter vector (chiral vector) $\overrightarrow{A} = (m,l) = m\overrightarrow{d} + m\overrightarrow{b}$, where $\overrightarrow{d}$ and $\overrightarrow{b}$ are the basis vectors of graphene ($a = b = a_0 = 2.46$ Å). The diameter d of the SWCNT is given by $d = (a_0/\pi)\sqrt{m^2+l^2+ml}$ (hereafter equivalently are identified by (m,l), where $m \geq l \geq 0$). One of the most striking characteristics of SWCNTs is that its intrinsic electrical property depends on the chiral indices (m,l), namely when $m = l$ or $m - l$ is divisible by 3, (m,l)SWCNTs belong to the nonmagnetic metals, otherwise it is nonmagnetic semiconducting, except that the extremely small diameter's SWCNTs are all metallic.[19,20] Due to its fascinating thermal, mechanical, chemical, and electrical and magnetic properties,[22–34] SWCNTs have been applied to a wide range of scientific and technology fields, such as, chemical and biological sensors,[23–27] gas's purification and adsorption,[22] scanning probe microscopy tips,[30] as well as photo electronic devices[31–33] etc.

Extensive and in-depth study of graphene nanoribbons and SWCNTs also have aroused great research interest in h-BN nanosheets, BN Nanotube, and especially, BN nanoribbons

Department of Physics, Anhui University, Hefei 230039, Anhui, China. Fax: +86-551-65107999; Tel: +86-551-65106477; E-mail:loup@ahu.edu.cn

(BNNRs), such as, experimental and theoretical studies have confirmed that the pristine BNNRs are magnetic metals.[35,36] Note that both edges of the pristine graphene nanoribbons are terminated with C. However, both edges of the pristine zigzag edge BNNRs with n chains (n-ZBNNRs) are terminated with N and B, respectively, whose are respectively called as the N-edge and the B-edge. When the pristine n-ZBNNR is modified by H at the B-edge (n-ZBNNR-BH), it turns into intriguing half-metallicity.[37–39] It is known that the dangling bonds of pristine BNNRs are rather active and can be easily passivated. When the pristine n-ZBNNR is modified by H at both of the N-edge and B-edge (n-ZBNNR-1H1H, see Fig. 11), it turns into nonmagnetic semiconductor with indirect wide-band gap owing to the large ionic nature of N-B bonds. Moreover, as ribbon width n increases, the charge transfer from the B-edge to the N-edge increases. As a result, as n increases, its band gap decreases monotonically. However, for both N-edge and B-edge H-passivated armchair edge BNNR with n dimer lines (n-ABNNR-1H1H), its band gap is direct band gap, which shows oscillation behavior as n increases.[40–42] Similar to graphene nanoribbons, the electronic and magnetic properties of BN nanoribbons have been modified by the termination and passivation of edges,[43–47] the vacancy defects, impurity or molecular doping,[48–53] strain,[54] and hydrogenation,[55,56] as well as external electric fields.[40,57]

Recently, the hybrid structures of BNNRs and graphene nanoribbons have also been proposed,[58–66] such as the hybrid BN-C nanoribbons,[59–62,64–66] which is considered as graphene nanoribbons embedded in BN nanostructures and vice versa, show rich electronic and magnetic properties. Tang et al. find that the band gap and edge magnetism of the hybrid BN-C nanoribbons can be regulated by the BN/C ratio.[64] Dutta et al. have predicted intrinsic half-metallic hybrid C-BN nanoribbons.[65] Tang et al. have observed that in the C chain-doped half-bare ZBNNRs, as the doping proceeds gradually from the N-edge to the B-edge, without an external electric field, there are semiconducting $\rightarrow$ half-metallic $\rightarrow$ metallic transitions occur.[66] Du et al. have predicted that via hybrid connection between a graphene nanoribbon and a BNNR, the hybrid C-BN single-walled nanotubes can be produced.[58] They also have found that armchair $C_{0.5}(BN)_{0.5}$ SWNTs belong to gapless semiconductors, while zigzag $C_{0.5}(BN)_{0.5}$ SWNTs belong to narrow gap semiconductors, independent of tube diameter.

On the other hand, in order to overcome the question which a suspending or free-standing graphene nanoribbon is usually twisted fairly easily (a practical application bottleneck),[67–69] a hybrid structure, namely nZGNR-(m,m)SWCNT, is suggested by Lou.[70,71] He finds that the nZGNR-(m,m)SWCNTs belong to ferromagnetic spin semiconductors.[72] Naturally, one would ask whether it is possible to form hybridized structure of the (m,m)SWCNT and n-ZBNRN? Moreover, heretofore, the edge termination and passivation of n-ZBNRNs are done via atoms or functional groups,[43–47] such as, Wang et al. have reported that functional group $-C_2H$ passivation can significantly reduce the BNNRs's band gaps.[43] Krepel et al. have studied edge oxidation effects on the structural, as well as electronic and magnetic properties of n-ZBNRNs.[44] Zeng et al. have studied edge fluorination effects on electronic structures and transport properties of BNNRs.[46] Lopez-Bezanilla et al. have revealed that O-passivation and S-passivattion make n-BNNRs become metallic.[47] However, how the edge passivation, by a (m,m)SWCNT instead of H, O, and S atoms, influences the thermal and mechanical stabilities, electronic, and magnetic properties of the pristine n-ZBNNR is not clear.

Motivated by above issues, we systematically investigated the thermal and mechanical, spin transport, as well as electrical and magnetic properties of the (m,m)SWCNT functionalized n-ZBNNR, by using classical molecular dynamic (MD) simulations, standard spin-polarized density functional theory (DFT) calculations, as well as the first-principles nonequilibrium Green's function method.

The remainder of this paper is organized as follows. In Section 2, we briefly describe computational method details. In Section 3, we display and discuss the results calculated for the thermal and mechanical, spin transport, as well as electrical and magnetic properties of the (m,m)SWCNT functionalized n-ZBNNR, first the issue of the geometric structures, then band structures, band gaps, magnetic moments, and spin transport behaviors, as well as the thermal and mechanical stabilities, after that, we discuss these results. We conclude the paper in Section 4.

2 Computational methods

The DFT calculations, the FET simulation (using the nonequilibrium Green's function formalism[73]), and the transition state search (using the nudged elastic band (NEB) method[74]), within a generalized gradient approximation[75] were performed by using the version 3.7 of OPENMX code[76,77], which is based on norm-conserving Kleinman-Bylander pseudopotentials[78] generated with multireference energies and optimized pseudoatomic basis functions[79,80] with a kinetic energy cutoff of 300 Ry. The cutoff radius of 7 bohrs has been chosen for all the basis functions, namely, B7.0–$s^2p^1d^1$,C7.0-$s^2p^2d^1$, N7.0-$s^2p^3d^1$, and H7.0-s^1p^1. We adopted a supercell geometry where the length of a vacuum region along the nonperiodic direction (x-, y-directions) was 30 Å. $1\times1\times121$ k-point sampling points are adopted in the Brillouin zone integration.[81] The geometries were optimized until the Hellmann-Feynman forces were less than 10^{-4} Hartree/bohr and the energy was less than 10^{-8} Hartree.

In order to show the thermal and mechanical stabilities of the studied systems, the MD simulations were performed by

using the version 4.0 of GULP code,[84,85] in which the B-H, N-H, C-C, B-N, C-B, and C-N interactions were described by the generic Dreiding force field parameters.[87]

3 Results and discussion

3.1 Geometric structures

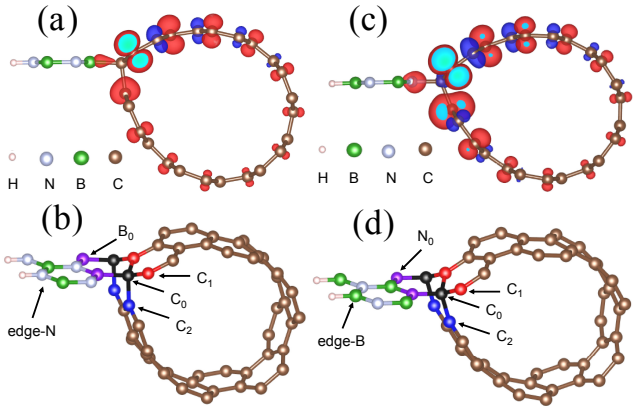

Fig. 1 Geometric structures and spatial distribution of the spin differences, (a) and (b) for 2ZBNNR-B-(6,6)SWCNT, whereas (c) and (d) for 2ZBNNR-N-(6,6)SWCNT. In spatial distribution of the spin differences, the red and blue surfaces represent the spin-up (↑) and spin-down (↓). The isosurface is 0.03 μ_B/Å^3. Geometric structures, in (b), the edge B site is marked by edge-B and the special N site is marked by N_0 (purple balls), whereas in (d), the special B site is marked by B_0 (purple balls) and the edge N site is marked by edge-N. Where C_0, C_1, and C_2, marked by the black, red, and blue respectively, are the special C sites.

It is noted that the both edges of the pristine *n*-ZBNNR are respectively terminated with N and B atoms and are called as the N-edge and the B-edge, respectively. Thus, the (*m*,*m*)SWCNT functionalized *n*-ZBNNRs have two different kind of forms. They are: (a) B-edge is bonded with (*m*,*m*)SWCNT while N-edge is modified with H (*n*ZBNNR-B-(*m*,*m*)SWCNT)), (b) N-edge is bonded with (*m*,*m*)SWCNT while B-edge is modified with H (*n*ZBNNR-N-(*m*,*m*)SWCNT). For example, the geometric structures of 2ZBNNR-B-(6,6)SWCNT and 2ZBNNR-N-(6,6)SWCNT are shown in Fig. 1. As shown in Fig. 1(b), in 2ZBNNR-B-(6,6)SWCNT, each C_0 possesses four nearest neighbor atoms, as a result, the C_0 and four nearest neighbor atoms form one C-B bond and three C-C bonds, namely, two C_0-C_1 bonds which bond distance is about 1.47 Å, one C_0-C_2 bond which bond distance is about 1.57 Å, and one C_0-B_0 bond which bond distance is about 1.61 Å, and hence, they belong to sp^3-hybridized. Similarly, in 2ZBNNR-N-(6,6)SWCNT (see Fig. 1(d)), each C_0 possesses four nearest neighbor atoms, as a result, the C_0 and four nearest neighbor atoms form one C-N bond and three C-C bonds, namely, two C_0-C_1 bonds which bond distance is about 1.50 Å, one C_0-C_2 bond which bond distance is about 1.55 Å, and one C_0-N_0 bond which bond distance is about 1.49 Å, and hence, they belong to sp^3-hybridized. It is clear that both 2ZBNNR-B-(6,6)SWCNT and 2ZBNNR-N-(6,6)SWCNT possess the sp^3-hybridized Y-shape and remaining tube-shape stability structures, which is the origin of its thermal and mechanical stabilities.

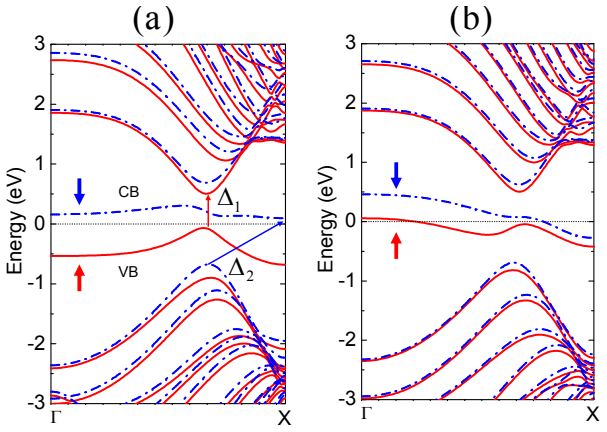

Fig. 2 Band structures, (a) for 2ZBNNR-N-(6,6)SWCNT, and (b) for 2ZBNNR-B-(6,6)SWCNT. Where the red solid and blue dash dotted lines denote the spin-up (↑) and spin-down (↓) bands, respectively. The Fermi level is set to zero. In (a), the common conduction band is marked by "CB", whereas the common valence band is marked by "VB". Δ_1 represents the spin-up channel's gap, and Δ_2 represents the spin-down channel's gap.

3.2 Band structures

Fig. 2(a) and 2(b) plot the band structures for 2ZBNNR-B-(6,6)SWCNT and 2ZBNNR-N-(6,6)SWCNT, respectively. As shown in Fig. 2(a), in 2ZBNNR-N-(6,6)SWCNT, each spin channel possesses different band gaps, where Δ_1 represents the spin-up channel's gap and Δ_2 represents the spin-down channel's gap. Fascinatingly, the common conduction band (CB) is spin-down channel, whereas the common valence band (VB) is spin-up channel. As a result, a common band gap (Δ_0) appears. In addition, from Fig. 1(c) and 4(b), one can find that each C_1, C_2, and N_0 possesses relatively large magnetic moments with same spin orientation, resulting in total magnetic moment of about 1 μ_B per unit cell. Note that when $\Delta_0 = 0$, it turns into a spin-gapless semiconductor.[88] Therefore, the 2ZBNNR-N-(6,6)SWCNT belongs to ferromagnetic intrinsic spin-semiconductors.[72] As for 2ZBNNR-B-(6,6)SWCNT, from Fig. 2(b), one can find that the 2ZBNNR-B-(6,6)SWCNT is a metal due to its spin-up and spin-down channels crossing the Fermi level. Moreover,

from Fig. 1(a) and 4(a), one can find that each C_1, C_2, and B_0 possesses relatively large magnetic moments with same spin orientation, resulting in total magnetic moment of about 0.56 μ_B per unit cell (see Table 2). Thus, the 2ZBNNR-B-(6,6)SWCNT is a intrinsic ferromagnetic metal.

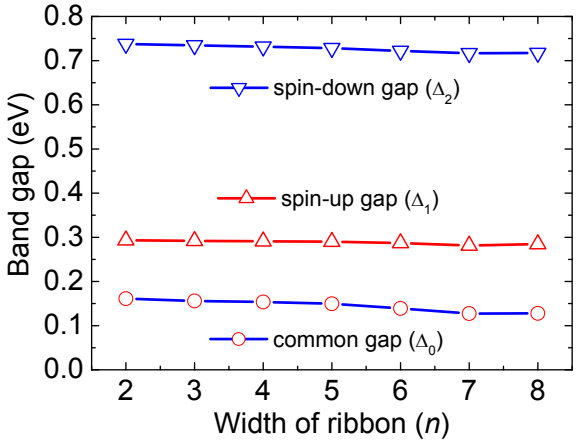

Fig. 3 *n*ZBNNR-N-(6,6)SWCNT' Δ_0, Δ_1, and Δ_2 as a function of n.

Table 1 Common band gap (Δ_0), spin-up band gap (Δ_1), and spin-down band gap (Δ_2) in the unit of eV for 8ZBNNR-N-(m,m)SWCNT.

8ZBNNR-N-(m,m)	Δ_0	Δ_1	Δ_2
8ZBNNR-N-(4,4)	0.146	0.393	1.054
8ZBNNR-N-(6,6)	0.128	0.285	0.717
8ZBNNR-N-(9,9)	0.138	0.199	0.513

3.3 Band gaps

For *n*ZBNNR-N-(6,6)SWCNT, at a given (m,m)=(6,6), Δ_0, Δ_1 and Δ_2 as a function of n are shown in Fig. 3. Remarkably, Δ_0, Δ_1 and Δ_2 are also essentially independent of n, which is different from that of *n*ZGNR-(6,6)SWCNT.[70] On the other hand, at a given $n = 8$, for 8BNNR-N-(m,m)SWCNT, Δ_0, Δ_1 and Δ_2 versus the tube diameter (m,m) are filled in Table 1. It is clear that Δ_1 and Δ_2 decrease with increasing (m,m), while Δ_0 change a little. This is because in the *n*ZBNNR-N-(m,m)SWCNT, the orbital composition of its band edge states are all originated from the atoms of -N-(m,m)SWCNT (see Fig. 9). However, in the *n*ZGNR-(m,m)SWCNT (see Fig. 14), the orbital composition of its band edge states are originated from the atoms of -(m,m)SWCNT as well as the edge atoms of *n*ZGNR, and as a result, its bang gap (Δ_0, Δ_1 and Δ_2) depends on n, as well as (m,m).[70]

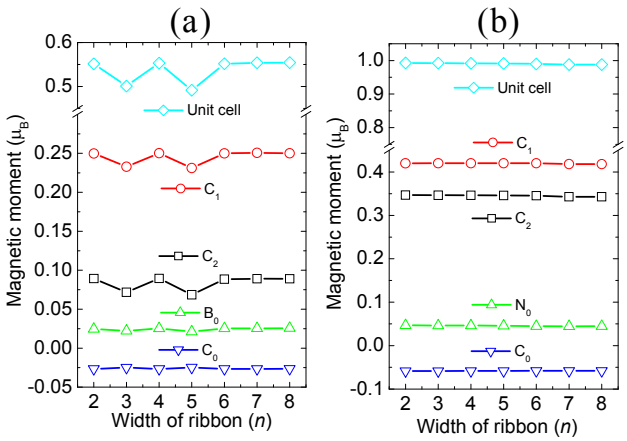

Fig. 4 Local magnetic moment as a function of n, (a) each C_0, C_1, C_2, B_0 atom, and per unite cell, for *n*ZBNNR-B-(6,6)SWCNTs; (b) each C_0, C_1, C_2, N_0 atom, and per unite cell, for *n*ZBNNR-N-(6,6)SWCNTs. Corresponding geometric structures refer to Fig. 1.

Table 2 The magnetic moments on each C_0, C_1, C_2 and B_0 atom, as well as per unite cell, in the unit of μ_B for 8ZBNNR-B-(m,m)SWCNT.

8ZBNNR-B-(m,m)	C_0	C_1	C_2	B_0	Cell
8ZBNNR-B-(4,4)	−0.032	0.267	0.155	0.021	0.636
8ZBNNR-B-(6,6)	−0.026	0.250	0.089	0.026	0.554
8ZBNNR-B-(9,9)	−0.025	0.252	0.080	0.033	0.543

3.4 Magnetic moments

Fig. 4(a) presents the magnetic moments on each C_0, C_1, C_2 and B_0 atom, as well as per unite cell, for *n*ZBNNR-B-(6,6)SWCNTs, as a function of n. One can find that at first the magnetic moments on each C_0, C_1, C_2 and B_0 atom exhibit oscillation with increasing n, while when $n \geq 6$, they are essentially independent of n. However, in contrast to *n*ZBNNR-B-(6,6)SWCNTs, the magnetic moments of *n*ZBNNR-N-(6,6)SWCNTs are essentially independent of n (Fig. 4(b)). On the other hand, at a given $n = 8$, for 8BNNR-B-(m,m)SWCNT, the magnetic moments on each C_0, C_1, C_2 and B_0 atom, as well as per unite cell versus the tube diameter (m,m) are filled in Table 2. It is clear that the magnetic moments on each C_0, C_1, C_2 and B_0 atom, as well as per unite cell are essentially independent of (m,m). In addition, from Fig. 4 and Table 2, one can find that in both *n*ZBNNR-B-(m,m)SWCNTs and *n*ZBNNR-N-(m,m)SWCNTs, each C_0 has negative moment, whereas its four neighbors have positive moment, such as, in *n*ZBNNR-B-(m,m)SWCNTs, the magnetic moment of each C-0 is spin-down, but the magnetic moments of its four neighbors (B_0, C_2, and two C_1) are spin-up.

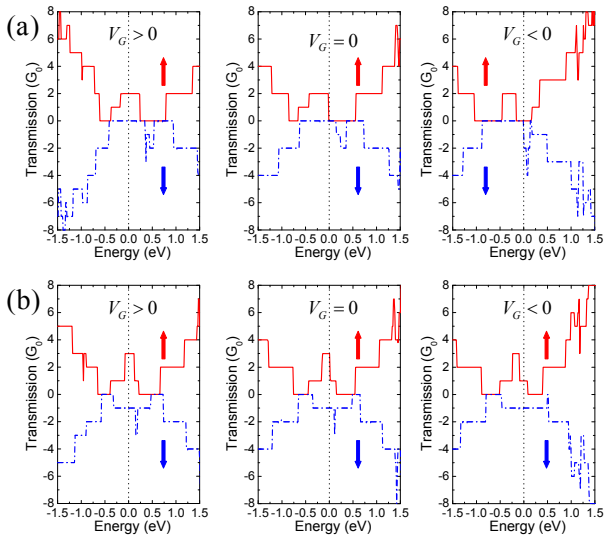

Fig. 5 Transmission coefficients versus gate voltage (V_g) under zero bias, (a) 5ZBNNR-N-(6,6)SWCNT FET, (b) 5ZBNNR-B-(6,6)SWCNT FET, where $G_0 = e^2/h$. The other marks are same as in Fig. 2.

In other words, the magnetic moments between each C_0 and four neighbor atoms adopt antiparallel spin orientation, which satisfies a design rule.[8]

3.5 Spin transport behaviors

In order to display spin transport behaviors of (m,m)SWCNT functionalized n-ZBNNR FET,[89] we calculate transmission coefficients versus gate voltage (V_g) under zero bias. The results are shown in Fig. 5(a) and 5(b) for 5ZBNNR-N-(6,6)SWCNT FET and 5ZBNNR-B-(6,6)SWCNT FET, respectively. From Fig. 5(a), one can find that when $V_g = 0$, the spin-up transmission coefficient $T_{\rm up}$ at the Fermi level, as well as the spin-down transmission coefficient $T_{\rm down}$, is zero, resulting in the relative spin polarization $\zeta = 0$ (defined as $\zeta = \frac{T_{\rm up} - T_{\rm down}}{T_{\rm up} + T_{\rm down}}$,[82,90,91] noting that the two particular values of ζ (=0 and ± 1) denote the completely unpolarized (CUP) and fully polarization, (FP) states, respectively). Whereas $V_g > 0$, around the Fermi level, the spin-up transmission coefficient $T_{\rm up}$ increases from 0 to 2 G_0 ($G_0 = e^2/h$), but the spin-down transmission coefficient $T_{\rm down}$ remains unchanged (0 G_0), resulting in $\zeta = 1$, namely, the FP current with spin-up goes through the 5ZBNNR-N-(6,6)SWCNT FET. When $V_g < 0$, on the other hand, around the Fermi level, the spin-up transmission coefficient $T_{\rm up}$ remains unchanged (0 G_0), but the spin-down transmission coefficient $T_{\rm down}$ increases from 0 to 2 G_0, resulting in $\zeta = -1$, namely, the FP current with spin-down goes through the 5ZBNNR-N-(6,6)SWCNT FET.

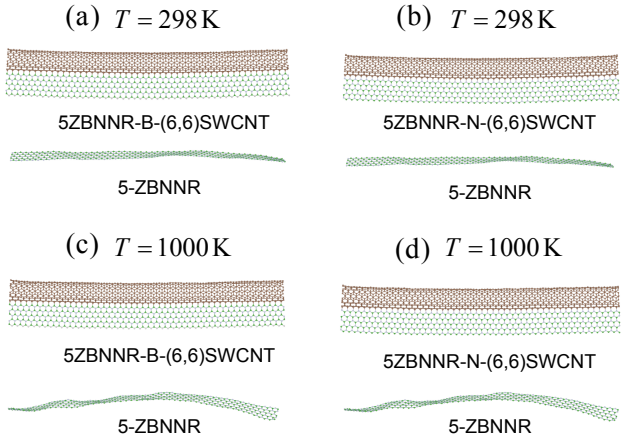

Fig. 6 Typical candid photos at 298 K and 1000 K, respectively, (a) and (c) for 5ZBNNR-B-(6,6)SWCNT, and (b) an (d) for 5ZBNNR-N-(6,6)SWCNT.

Interestingly, in 5ZBNNR-B-(6,6)SWCNT FET, as shown in Fig. 5(b), when $V_g = 0$, around the Fermi level, the spin-up transmission coefficient $T_{\rm up}$, as well as the spin-down transmission coefficient $T_{\rm down}$, is 1 G_0, resulting in $\zeta = 0$, namely, there is only CUP current through 5ZBNNR-B-(6,6)SWCNT FET. Whereas $V_g > 0$, around the Fermi level, the spin-up transmission coefficient $T_{\rm up}$ increases from 1 to 3 G_0, but the spin-down transmission coefficient $T_{\rm down}$ remains unchanged (1 G_0), resulting in $\zeta = 0.75$, namely, 75% spin-up polarization current goes through the 5ZBNNR-B-(6,6)SWCNT FET. When $V_g < 0$, on the other hand, around the Fermi level, the spin-up transmission coefficient $T_{\rm up}$, as well as the spin-down transmission coefficient $T_{\rm down}$, is 1 G_0, resulting in $\zeta = 0$, namely, there is only CUP current through 5ZBNNR-B-(6,6)SWCNT FET.

3.6 Thermal and mechanical stabilities

Fig. 6 shows the results of the MD simulations for 5-ZBNNR, 5ZBNNR-B-(6,6)SWCNT, and 5ZBNNR-N-(6,6)SWCNT, which were performed in the NVT ensemble, by 10^6 MD steps with a time step of 0.5 fs, at 298 and 1000 K, respectively. It is clear that the 5ZBNNR-N-(6,6)SWCNT, as well as the 5ZBNNR-B-(6,6)SWCNT, does not wrinkle even at 1000 K (Fig. 6(c) and 6(d)). However, at 298 K the 5-ZBNNR is already wrinkled (Fig. 6(a) and 6(b)). These results show that the sp^3-hybridized Y-shape and remaining tube-shape stability structure commonly used for building construction that the (m,m)SWCNT functionalized n-ZBNNR entails much greater flexural rigidity than a n-ZBNNR.

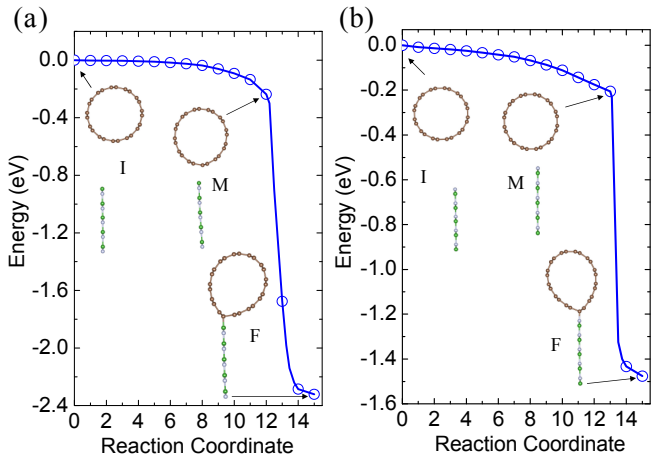

Fig. 7 The minimal energy path, where mark I, M, and F, respectively, represent initial, middle, and final states along the minimal energy path, (a) for formed pristine 5ZBNNR-B-(6,6)SWCNT and (b) for formed pristine 5ZBNNR-N-(6,6)SWCNT.

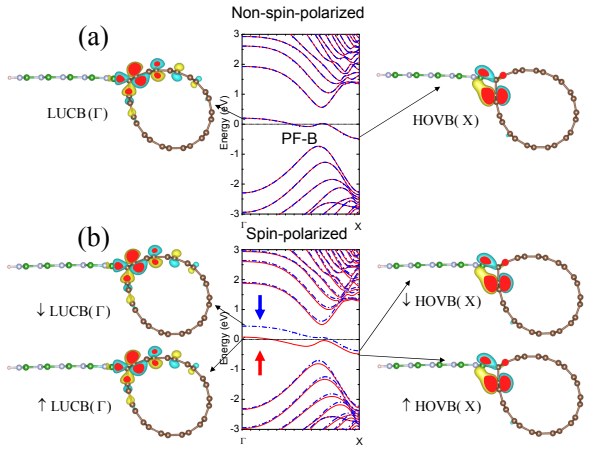

Fig. 8 Nor-spin-polarized structure and spin-polarized band structure with partial charge densities of the lowest unoccupied conduction band (LUCB), as well as the highest occupied valence band (HOVB), near the Γ and X points for 5ZBNNR-B-(6,6)SWCNT. (a) Nor-spin-polarized structure with partial charge densities in the paramagnetic state. A partial-filled band (PF-B) across the Fermi level is marked by "PF-B". (b) Ferromagnetic state's band structure with partial charge densities. The isosurface of 0.05 e/Å^3 is adopted. The other marks are same as in Fig. 2.

3.7 Synthetic route

Here, a simple two-step synthetic route for the preparation of (m,m)SWCNT functionalized n-ZBNNRs from n-ZBNNR and (m,m)SWCNT is presented. Firstly, we synthesize pristine (m,m)SWCNT functionalized n-ZBNNRs, and then the pristine (m,m)SWCNT functionalized n-ZBNNRs are modified by H, we get (m,m)SWCNT functionalized n-ZBNNRs. For example, a pristine 5ZBNNR-B-(6,6)SWCNT, as well as a pristine 5ZBNNR-N-(6,6)SWCNT, can be assembled through the edge of a pristine 5-ZBNNR vertically absorbed on the side wall of (6,6)SWCNT. Then, the pristine 5ZBNNR-B-(6,6)SWCNT is modified by H, we get 5ZBNNR-B-(6,6)SWCNT, while the pristine 5ZBNNR-N-(6,6)SWCNT is modified by H, we get 5ZBNNR-N-(6,6)SWCNT. On the other hand, from Fig. 7(a) and 7(b), one can find that pristine 5-ZBNNR and (6,6)SWCNT formed the pristine 5ZBNNR-B-(6,6)SWCNT or the pristine 5ZBNNR-N-(6,6)SWCNT does not need any activation energy. Moreover, the formation energies of pristine SWCNT functionalized n-ZBNNRs are always less than zero, such as the pristine 5ZBNNR-B-(6,6)SWCNT is about −2.32 eV, and the pristine 5ZBNNR-N-(6,6)SWCNT is about −1.48 eV. Therefore, the pristine 5ZBNNR-B-(6,6)SWCNT and pristine 5ZBNNR-N-(6,6)SWCNT not only are steady, but also can be spontaneously formed. In addition, the conformation of the pristine 5ZBNNR-B-(6,6)SWCNT is more energetically favorable than the conformation of pristine the 5ZBNNR-N-(6,6)SWCNT.

3.8 Origin of electronic and magnetic properties

In order to explore the origin of the electronic and magnetic properties of the SWCNT functionalized BN nanoribbons, for 5ZBNNR-B-(6,6)SWCNT, the nor-spin-polarized band structure and spin-polarized band structure with corresponding partial charge densities of the lowest unoccupied conduction band (LUCB), as well as the highest occupied valence band (HOVB), near the Γ and X points are calculated and are displayed in Fig. 8. From Fig. 8(a), one can find that at the Fermi level, there is a partial-filled band (PF-B). Such PF-B is the source of the 5ZBNNR-B-(6,6)SWCNT's magnetism.[92,94] Note that both N-edge and B-edge of 5-ZBNNR-1H1H are modified by H (Fig. 13),[93] whereas, in the 5ZBNNR-B-(6,6)SWCNT, N-edge is modified by H, but B-edge is functionalized with a (6,6)SWCNT instead of H (B-edge of 5-ZBNNR-NH through C_0 bonding with −(6,6)SWCNT, refer to Fig. 1(b)). Thus, such PF-B is originated from the special edge shape of 5ZBNNR-B-(6,6)SWCNT. Indeed, as shown in Fig. 8(a), the PF-B marked by HOVB(X), as well as marked by LUCB(Γ), is contributed mainly by the atom orbitals of −(6,6)SWCNT which are absent in the 5-ZBNNR-1H1H. On the other hand, the PF-B corresponds to electron states localized and makes the system occur spin symmetry breaking.[92,94] As shown in Fig. 8(b), now there are two bands across the Fermi level, namely, (i) the spin-up band

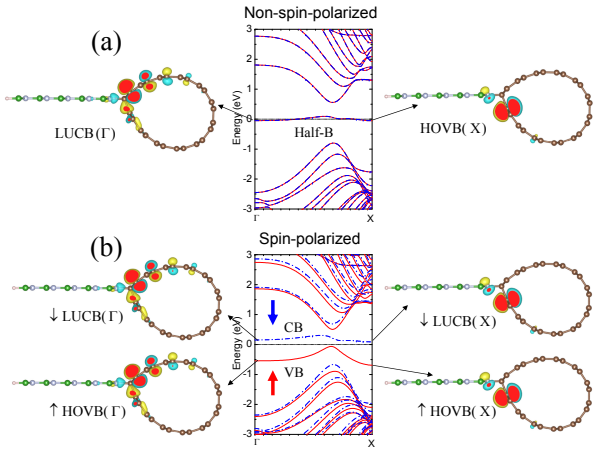

Fig. 9 Nor-spin-polarized structure and spin-polarized band structure with partial charge densities of the LUCB, as well as HOVB for the 5ZBNNR-N-(6,6)SWCNT. (a) Nor-spin-polarized structure with partial charge densities in the paramagnetic state, where a half-filled flat band is marked by "Half-B". (b) Ferromagnetic state's band structure with partial charge densities. The other marks are same as in Fig. 8.

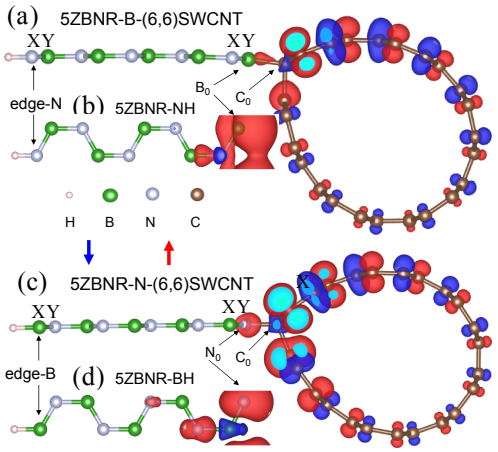

Fig. 10 Spatial distribution of the spin differences: (a) 5ZBNNR-B-(6,6)SWNT, (b) Each edge-N atom of 5-ZBNNR is passivated with H atom (5-ZBNNR-NH), (c) 5ZBNNR-N-(6,6)SWNT, and (d) 5-ZBNNR-BH. "X" and "Y" mark different sublattice, namely, X-sublattice, Y-sublattice. The other marks are same as in Fig. 1, except that the isosurface is 0.015 $\mu_B/Å^3$, instead of 0.03 $\mu_B/Å^3$, for spin-down (↓).

marked with ↑LUCB(Γ) and ↑HOVB(X), (ii) the spin-down band marked with ↓LUCB(Γ) and ↓HOVB(X). As a result, the magnetism appears in the 5ZBNNR-B-(6,6)SWCNT. Thus, the 5ZBNNR-B-(6,6)SWCNT is a ferromagnetic metal.

As for 5ZBNNR-N-(6,6)SWCNT, from Fig. 9(a), one can find that at the Fermi level there is a half-filled flat band (Half-B). Such Half-B is the source of the 5ZBNNR-N-(6,6)SWCNT's magnetism.[92,94] In contrast to the case of the 5ZBNNR-B-(6,6)SWCNT, in the case of the 5ZBNNR-N-(6,6)SWCNT, B-edge is modified by H instead of a (6,6)SWCNT, but N-edge is functionalized with a (6,6)SWCNT instead of H (N-edge of 5-ZBNNR-BH through C_0 bonding with −(6,6)SWCNT, refer to Fig. 1(d)). Indeed, as shown in Fig. 9(a), the calculated partial charge densities of the LUCB(Γ) and HOVB(X) show that the Half-B is contributed mainly by the atom orbitals of −(6,6)SWCNT which are absent in the 5-ZBNNR-1H1H. On the other hand, such Half-B corresponds to electron states localized and makes the system occur spin symmetry breaking.[92,94] Indeed, as shown in Fig. 9(b), near the Fermi level there are two bands to appear, namely, (i) the spin-up band marked with "VB", (ii) the spin-down band marked with "CB". Thus, the 5ZBNNR-N-(6,6)SWCNT belongs to ferromagnetic intrinsic spin-semiconductors.

3.9 Understanding of ferromagnetism

The ferromagnetic properties of *n*ZBNNR-B-(*m*,*m*)SWCNTs and *n*ZBNNR-N-(*m*,*m*)SWCNTs can be better to understand by using a design rule.[8] For example, the 5ZBNNR-N-(6,6)SWCNT can be viewed as a BNNR coupled with a graphene nanoribbon shown in Fig. 10(c). On the left, there is a 5-ZBNNR-BH, which one edge is on the X-sublattice (H-passivated edge-B atom shown in Fig. 10(c)) and the other edge is on Y-sublattice (N_0 atom shown in Fig. 10(c)). The two edges must be antiferromagnetic coupled, according to the design rule. However, because the local spin moment on the edge-B (belong to X-sublattice) is completely destroyed due to each edge-B atom H passivation, the 5-ZBNNR-BH displays ferromagnetic, which is shown in Fig. 10(d). On the other hand, on the right, because the -(6,6)SWCNT connected with the 5-ZBNNR-BH via C_0, each C_0 has sp^3 hybridization with four nearest neighbor atoms (N_0, C_2 and two C_1 atoms, refer to Fig. 1(d)). Assume that each C_0 is removed, the -(6,6)SWCNT that C_0 atoms have been removed can be viewed as curved graphene nanoribbon, except that two edges belong to the same Y-sublattice (C_1 and C_2 atoms). According to the design rule, the curved graphene nanoribbon's two edges should be ferromagnetic coupled. Therefore, on the left, there is a flat ferromagnetic BNNR (5-ZBNNR-BH), and on the right, there is a ferromagnetic curved graphene nanoribbon (broken -(6,6)SWCNT). Note that the orientation of magnetic moment of C_0 atom should be different from that of its four neighbors (N_0, C_2, and two C_1 atoms). Thus, between the 5-ZBNNR-BH and curved graphene nanoribbon should be a ferromagnetic coupling shown in Fig. 10(c). Hence, 5ZBNNR-N-(6,6)SWCNT possesses a ferromagnetic ground state.

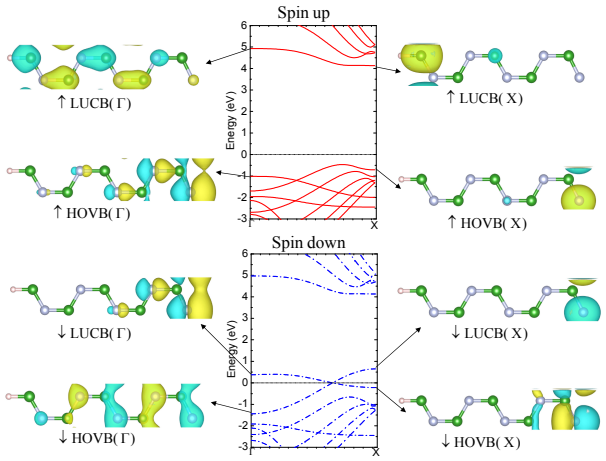

Fig. 11 The band structures of the 5-ZBNNR-BH in the ferromagnetic state with partial charge densities of the LUCB, as well as HOVB. The other marks are same as in Fig. 8.

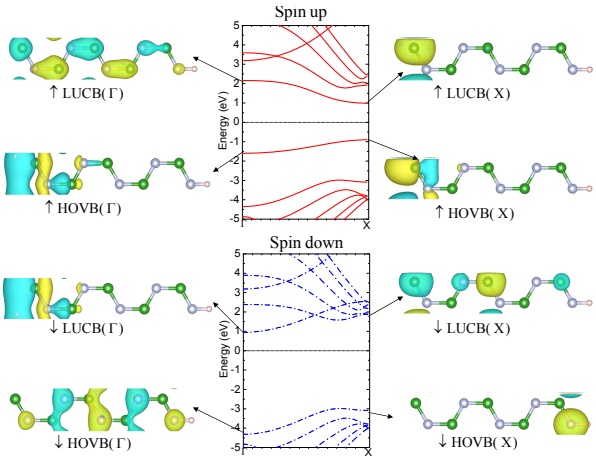

Fig. 12 The spin-polarized band structures of the 5-ZBNNR-NH in the ferromagnetic state with partial charge densities of the LUCB, as well as HOVB. The other marks are same as in Fig. 8.

In addition, comparing the spatial distribution of the spin differences between 5ZBNNR-N-(6,6)SWCNT and 5-ZBNNR-BH (bare N-edge), namely comparing Fig. 10(d) with Fig. 10(c), one can find that after N-edge of 5-ZBNNR-BH bonded by a (6,6)SWNT, its magnetic properties occur to obviously change. Indeed, in pristine 5-ZBNNR-BH, each edge-N atom possesses a magnetic moment of 0.954 μ_B. While in 5ZBNNR-N-(6,6)SWCNT, each edge-N atom (N-0 atom) possesses only a magnetic moment of 0.05 μ_B (see Fig. 4(b)). In order to find out the reason of magnetic property change, for the 5-ZBNNR-BH, the ferromagnetic state's band structure and with corresponding partial charge densities of the LUCB, as well as HOVB, at the Γ and X points are calculated and are displayed in Fig. 11. One can find that ↑HOVB(Γ), ↓LUCB(Γ), and ↓HOVB(X) correspond to a dangling-bond state at the N-edge and are strongly affected by the passivation. In contrast, ↑HOVB(X) and ↓LUCB(X) correspond to the usual lone-pair state of a threefold coordinated nitrogen and are hardly affected by the passivation. Indeed, from Fig. 9, one can find that the original dangling bond states of 5-ZBNNR-BH have been removed by (6,6)SWCNT passivation, which is similar to H passivation. On the other hand, in contrast to the H passivation, where the H passivation destroys the local spin moment on the edge-N atom completely (see Fig. 13), the (6,6)SWCNT passivation reduces the local spin moment of each edge-N atom from 0.954 to 0.05 μ_B.

Similarly, 5ZBNNR-B-(6,6)SWCNT can be viewed as a BNNR coupled with a graphene nanoribbon. On the left, there is a 5-ZBNNR-NH, which one edge is on the X-sublattice (H-passivated edge-N atom shown in Fig. 10(a)) and the other edge is on Y-sublattice (B_0 atom). According to the design rule,[8] the two edges must be antiferromagnetic coupled. However, because the local spin moment on the edge-N (belong to X-sublattice) is completely destroyed by each edge-N atom H passivation, the 5-ZBNNR-NH displays ferromagnetic, as shown in Fig. 10(b). On the other hand, on the right, because the -(6,6)SWCNT connected with the 5-ZBNNR-NH via C_0, each C_0 has sp^3 hybridization with four nearest neighbor atoms (B_0, C_2 and two C_1 atoms, refer to Fig. 1(b)). Assume that each C_0 is removed, the -(6,6)SWCNT that C_0 have been removed can be viewed as curved graphene nanoribbon, except that two edges belong to the same Y-sublattice (C_1 and C_2 atoms). According to the design rule, the curved graphene nanoribbon's two edges should be ferromagnetic coupled. Therefore, on the left, there is a flat ferromagnetic BNNR (5-ZBNNR-NH), and on the right, there is a ferromagnetic curved graphene nanoribbon (broken -(6,6)SWCNT). Note that the orientation of magnetic moment of C_0 atoms should be different from that of its four neighbors (B_0, C_2, and two C_1 atoms). Thus, between the 5-ZBNNR-NH and curved graphene nanoribbon should be a ferromagnetic coupling, as shown in Fig. 10(a). Hence, 5ZBNNR-B-(6,6)SWCNT possesses a ferromagnetic ground state.

In addition, by comparing Fig. 10(a) with Fig. 10(b), one can find that after B-edge of 5-ZBNNR-NH bonded by a (6,6)SWNT, obviously its magnetic properties occur to change. Indeed, in 5-ZBNNR-NH, each edge-B atom possesses a magnetic moment of 1.014 μ_B. While in 5ZBNNR-B-(6,6)SWCNT, each edge-B atom (B_0 atom) possesses only a magnetic moment of 0.025 μ_B (see Fig. 4(a)). This is due to that the original dangling bond states of the 5-ZBNNR-NH have been removed by (6,6)SWCNT passivation. Indeed, from Fig. 12, one can find the ↑HOVB(Γ), ↑HOVB(X), and ↓LUCB(Γ), which correspond to a dangling-bond state at the

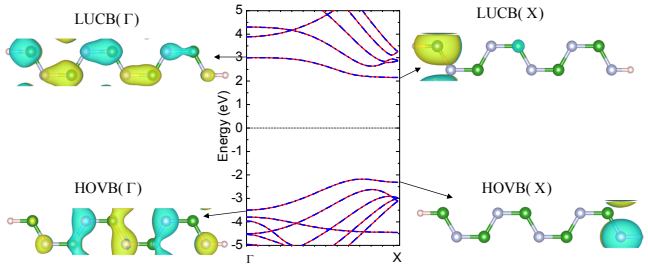

Fig. 13 The band structure of 5-ZBNNR-1H1H, and partial charge densities of the LUCB, as well as HOVB, at the Γ and X points. The other marks are same as in Fig. 8.

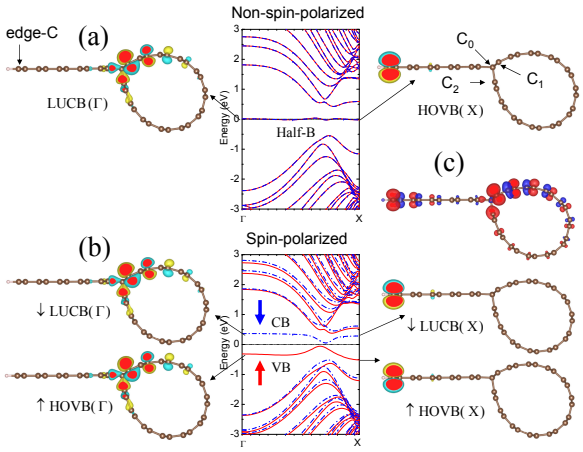

Fig. 14 Band structures with spatial distribution of the spin differences, and corresponding partial charge densities of the LUCB, as well as HOVB, for 5ZGNR-(6,6)SWCNT. (a) Nor-spin-polarized structure with corresponding partial charge densities in the paramagnetic state, where a half-filled flat band is marked with "Half-B". (b) ferromagnetic state's band structure with corresponding partial charge densities, and (c) spatial distribution of the spin difference. The other marks are same as in Fig. 8.

B-edge. While in Fig. 8, the corresponding dangling-bond state is completely removed by the (6,6)SWCNT passivation. Meanwhile, the (6,6)SWCNT passivation reduces the local spin moment of each edge-B atom from 1.014 to 0.025 μ_B.

3.10 Differences between SWCNT and H passivations

In order to further study the differences between (6,6)SWCNT and H passivations, the band structure with partial charge densities of the LUCB, as well as HOVB, at the Γ and X points of the 5-ZBNNR-1H1H are calculated and are shown in Fig. 13. By comparing Fig. 11 with Fig. 13, one can find that after each edge-N atom of 5-ZBNNR-BH is bonded by H, that ↓LUCB(X) and ↑HOVB(X) correspond to the edge state localized at edge-N atoms is still remained as shown in Fig. 13 (HOVB(X)), while that ↑HOVB(Γ), ↓LUCB(Γ), and ↓HOVB(X) correspond to the dangling-bond state at the N-edge is completely removed. Meanwhile, the local spin moment on each edge-N atom vanishes. By comparing Fig. 13 with Fig. 12, we find that after each edge-B atom of 5-ZBNNR-BH is modified by H, that ↑LUCB(X) corresponds to the edge state localized on edge-B atoms is still remained as shown in Fig. 13 (LUCB(X)), while that ↑HOVB(Γ) and ↑HOVB(X), as well as ↓LUCB(Γ) correspond to the dangling-bond state at the B-edge is completely removed. Meanwhile, the local spin moment at each edge-B atom vanishes.

Noted that both *n*ZGNR-(m,m)SWCNT and *n*ZBNNR-N-(m,m)SWCNT[70,71] are intrinsic spin semiconductors. Therefor, it is interesting to compare the electronic and magnetic properties between *n*ZBNNR-N-(m,m)SWCNT and *n*ZGNR-(m,m)SWCNT. Fig. 14 shows band structures with spatial distribution of the spin differences, and partial charge densities of the LUCB, as well as HOVB, at the Γ and X points for 5ZGNR-(6,6)SWCNT. By comparing Fig. 9 with Fig. 14, one can find that both 5ZBNNR-N-(6,6)SWCNT and 5ZGNR-(6,6)SWCNT have very similar band structures, except that for spin up channel, the band gap of 5ZBNNR-N-(6,6)SWCNT is direct, whereas, the band gap of 5ZGNR-(6,6)SWCNT is indirect. However, by comparing Fig. 10(c) with Fig. 14(c), one can find that there are obviously differences in their local magnetic moment distributions, such as in 5ZBNNR-N-(6,6)SWCNT, each C_1, C_2, and N_0 has a relatively large local magnetic moment (Fig. 10(c)), whereas in 5ZGNR-(6,6)SWCNT, in addition to C_1 and C_2, each edge-C by H passivation also has a relatively large local magnetic moment (Fig. 14(c)). This is due to that in 5ZGNR-(6,6)SWCNT, the edge state localizes at edge-C atoms with H passivation (HOVB(X), ↑HOVB(X), and ↓LUCB(X), as shown in Fig. 14(a-b)) and leads corresponding local spin moment on the edge-C atoms with H passivation. However, in 5ZBNNR-N-(6,6)SWCNT, the edge state localizes at N_0 atom (belong to original 5-ZBNNR-BH) and C_2 atom (belong to original (6,6)SWCNT) (HOVB(X), ↑HOVB(X), and ↓LUCB(X), as shown in Fig. 9(a-b)) and leads corresponding local spin moment on the N_0 and C_2 atoms.

3.11 Understanding of band gap change

From Fig. 9(b), one can find that both "CB" and "VB" of 5ZBNNR-N-(6,6)SWCNT are all originated from the atom orbitals of -N-(6,6)SWCNT. However, in 5ZGNR-(6,6)SWCNT (see Fig. 14(b)), near at Γ point, its "CB" and "VB" are originated from the atom orbitals of -(6,6)SWCNT, but near at X point, its "CB" and "VB" are originated from the atom orbitals of the edge-B atom. This is reason that the band

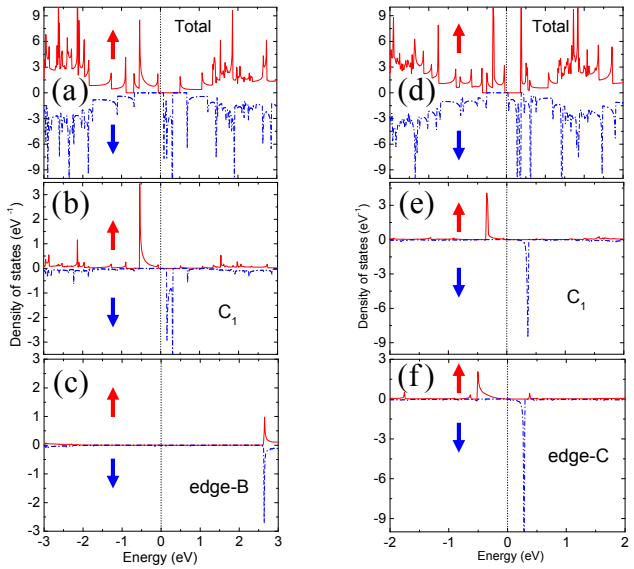

Fig. 15 Total density of states and the LDOS of the edge atom and C_1 atom. (a-c) for 5ZGNR-N-(6,6)SWCNT. (d-f) for 5ZGNR-(6,6)SWCNT. The other marks are same as in Fig. 8.

gap change of *n*ZBNNR-N-(m,m)SWCNT is different from that of *n*ZGNR-(m,m)SWCNT. In order to further verify this conclusion, we calculate total density of states and the LDOS of the edge atoms and C_1 atom for 5ZBNNR-N-$(6,6)$SWCNT and 5ZGNR-$(6,6)$SWCNT systems, respectively. The results are shown in Fig. 15. Indeed, by comparing Fig. 15(a) with Fig. 15(b) and Fig. 15(c), one can find that in 5ZBNNR-N-$(6,6)$SWCNT, the band edge states are contributed by the C_1 atom of (m,m)SWCNT (Fig. 15(b)), whereas the edge-B atom of 5ZBNNR only contributes to the hight energy band state (Fig. 15(c)). As a result, the bang gap of *n*ZBNNR-N-(m,m)SWCNT changes with (m,m), but is independent of *n*. However, by comparing Fig. 15(d) with Fig. 15(e) and Fig. 15(f), one can find that in 5ZGNR-$(6,6)$SWCNT, the band edge states are contributed not only by the C_1 atom of (m,m)SWCNT (Fig. 15(e)), but also by the edge-C atom of 5ZGNR (Fig. 15(f)). As a result, the bang gap of *n*ZGNR-(m,m)SWCNT depends on both *n* and (m,m).[70]

4 Conclusion

Based upon MD simulations, DFT calculations, as well as the first-principles nonequilibrium Green's function method, we have been predicted the (m,m)SWCNT functionalized *n*-ZBNNRs, namely, *n*ZBNNR-B-(m,m)SWCNTs and *n*ZBNNR-N-(m,m)SWCNTs. The DFT calculations reveal that there is no any activation barrier in the processes of pristine *n*ZBNNR-B-(m,m)SWCNTs and *n*ZBNNR-N-(m,m)SWCNTs formed. Moreover, the formation energies of pristine SWCNT functionalized *n*-ZBNNRs are always less than zero, such as the pristine 5ZBNNR-B-(6,6)SWCNT is about -2.32 eV, and the pristine 5ZBNNR-N-(6,6)SWCNT is about -1.48 eV. Therefore, they not only are steady, but also can be spontaneously formed. Amazingly, regardless of *n* and (m,m), the *n*ZBNNR-B-(m,m)SWCNTs belong to the intrinsic ferromagnetic metals, whereas the *n*ZBNNR-N-(m,m)SWCNTs belong to the ferromagnetic intrinsic spin-semiconductors in which completely spin-polarized currents can be created and manipulated only just by applying a gate voltage. These unique electronic and magnetic properties are originated from the special edge shape of $-(m,m)$SWCNT, which have potential applications in nanoelectronics and spintronics.

Acknowledgements

This work was supported by the National Natural Science Foundation of China (grant no. 11174003) and the 211 Project of Anhui University.

References

1 Y.-W. Son, M. L. Cohen and S. G. Louie, *Phys. Rev. Lett.* 2006, **97**, 216803.
2 K. Nakada, M. Fujita, G. Dresselhaus and M. S. Dresselhaus, *Phys. Rev. B: Condens. Matter* 1996, **54**, 17954.
3 M. Fujita, K. Wakabayashi, K. Nakada and K. Peculiar. Kusakabe, *J. Phys. Soc. Jpn*. 1996, **65**, 1920-1923.
4 H. Lee, Y.-W. Son, N. Park, S. Han and J. Yu, *Phys. Rev. B: Condens. Matter* 2005, **72**, 174431.
5 Y.-W. Son, M. L. Cohen and S. G. Louie, *Nature* (London) 2006, **444**, 347-349.
6 W. Y. Kim and K. S. Kim, *Nature Nanotech*. 2008, **3**, 408-412.
7 T. B. Martins, A. J. R. da Silva, R. H. Miwa and A. Fazzio, *Nano Lett*. 2008, **8**, 2293-2298.
8 D. Yu, E. M. Lupton, M. Liu, W. Liu and F. Liu, *Nano Res*. 2008, **1**, 56-62.
9 D. Yu, E. M. Lupton, H. J. Gao, C. Zhang and F. Liu, *Nano Res*. 2008, **1**, 497-501.
10 D. -E. Jiang, B. G. Sumpter and Sheng. Dai, *J. Phys. Chem. B*, 2006, **110**, 23628-23632.
11 D. -E. Jiang, B. G. Sumpter and Sheng. Dai, *J. Chem. Phys*. 2007, **126**, 134701.
12 J.-I. Takashiro, Y. Kudo, S.-J. Hao, K. Takai, D. N. Futaba, T. Enoki and M. Kiguchi, *Phys. Chem. Chem. Phys*. 2014, **16**, 21363-21371.
13 O. Hod, V. Barone, J. E. Peralta and G. E. Scuseria, *Nano Lett*. 2007, **7**, 2295-2299.
14 E. -J. Kan, Z. Li, J. -L. Yang and J. G. Hou, *J. Am. Chem. Soc*. 2008, **130**, 4224-4225.

15 M. H. Wu, X. J. Wu and X. C. Zeng, *J. Phys. Chem. C*, 2010, **114**, 3937-3944.

16 D. Gunlycke, J. Li, J. W. Mintmire and C. T. White, *Appl. Phys. Lett.* 2007, **91**, 112108.

17 M. H. Wu, Y. Pei and X. C. Zeng, *J. Am. Chem. Soc.* 2010, **132**, 5554-5555.

18 S. Tang and X. Cao, Phys. *Chem. Chem. Phys.* 2014, **16**, 23214-23223.

19 L. -C. Qin, *Phys. Chem. Chem. Phys*. 2007, **9**, 31-48.

20 Z. Liu and L. -C. Qin, *Chem. Phys. Lett.* 2005, **408**, 75-79.

21 A. J. Du, S. C. Smith and G. Q. Lu, *Nano Lett.* 2007, **7**, 3349-3354.

22 L. Mandeltort, De-Li. Chen, W. A. Saidi, J. K. Johnson, M. W. Cole and J. T., Jr. Yates, *J. Am. Chem. Soc*. 2013, **135**, 7768-7776.

23 J. A. Robinson, E. S. Snow, S. C. Badescu, T. L. Reinecke and F. K. Perkins, *Nano Lett.* 2006, **6**, 1747-1751.

24 S. Boussaad, B. A. Diner and J. Fan, *J. Am. Chem. Soc.* 2008, **130**, 3780-3787.

25 M. E. Roberts, M. C. LeMieux and Z. Bao, *ACS Nano* 2009, **3**, 3287-3293.

26 M. B. Lerner, J. M. Resczenski, A. Amin, R. R. Johnson, J. I. Goldsmith and A. T. C. Johnson, *J. Am. Chem. Soc.* 2012, **134**, 14318-14321.

27 M. Dionisio, J. M. Schnorr, V. K. Michaelis, R. G. Griffin, T. M. Swager and E. Dalcanale, *J. Am. Chem. Soc*. 2012, **134**, 6540-6543.

28 S. M. Lee, K. H. An, Y. H. Lee, G. Seifert and T. Frauenheim, *J. Am. Chem. Soc.* 2001, **123**, 5059-5063.

29 B. Chakraborty, P. Modak and S. Banerjee, *J. Phys. Chem. C* 2012, **116**, 22502-22508.

30 J. H. Hafner, C. -L Cheung and C. M. Lieber, *J. Am. Chem. Soc.* 1999, **121**, 9750-9751.

31 W. A. Deheer, A. Chatelain and D. Ugarte, *Science* 1995, **270**, 1179-80.

32 C. -H. Liu, C. -C. Wu and Z. Zhong, *Nano Lett.* 2011, **11**, 1782-1785.

33 Y. Zhong, T. Kaneko, J. Kong, and R. Hatakeyama, *J. Am. Chem. Soc.* 2009, **131**, 3412-3413.

34 M. M. J. Treacy, T. W. Ebbesen and J. M. Gibson, *Nature* 1996, **381**, 678-680.

35 V. Barone and J. E. Peralta, *Nano Lett.* 2008, **8**, 2210-2214.

36 M. Terrones, J. C. Charlier, A. Gloter, E. Cruz-Silva, E. Terres, Y. B. Li, Z. Zanolli, J. M. Dominguez, H. Terrones, Y. Bando and D. Golberg, *Nano Lett.* 2008, **8**, 1026-1032.

37 F.Zheng, G. Zhou, Z. Liu, J. Wu, W. Duan, B. Gu and S. B. Zhang, *Phys. Rev. B: Condens. Matter* 2008, **78**, 205415.

38 L.Lai, J. Lu, L. Wang, G. F. Luo, J. Zhou, R. Qin, Z. X. Gao and W. N. Mei, *J. Phys. Chem. C* 2009, **113**, 2273-2276.

39 E. Kan, F. Wu, H. Xiang, J. Yang and M. -H. Whangbo, *J. Phys. Chem. C* 2011, **115**, 17252-17254.

40 Z. H. Zhang and W. L. Guo, *Phys. Rev. B: Condens. Matter* 2008, **77**, 075403.

41 M. Topsakal, E. Akturk and S. Ciraci, *Phys. Rev. B: Condens. Matter* 2009, **79**, 115442.

42 R. Mukherjee and S. Bhowmick, *J. Chem. Theory Comput.* 2011, **7**, 720-724.

43 Y.Wang, Y. Li and Z. Chen, *J. Phys. Chem. C* 2014, **118**, 25051-25056.

44 D. Krepel and O. Hod, *J. Chem. Theory Comput.* 2014, **10**, 373-380.

45 A. Lopez-Bezanilla, J. Huang, H. Terrones, B. G. Sumpter, *J. Phys. Chem. C* 2012, **116**, 15675-15681.

46 J. Zeng, K.-Q. Chen and C. Q. Sunb, *Phys. Chem. Chem. Phys.*, 2012, **14**, 8032-8037.

47 A. Lopez-Bezanilla, J. Huang, H. Terrones and B. G. Sumpter, *Nano Lett.* 2011, **11**, 3267-3273.

48 G. Yu, D. Liu, W. Chen, H. Zhang and X. Huang, *J. Phys. Chem. C* 2014, **118**, 12880-12889.

49 D. Ghosh, P. Parida and S. K. Pati, *J. Phys. Chem. C* 2014, **118**, 14670-14676.

50 D. Ghosh, P. Parida and S. K. Pati, *J. Mater. Chem. C*, 2014, **2**, 392-398.

51 S. Tang and S. Zhang, *J. Phys. Chem. C* 2013, **117**, 17309-17318.

52 W. Chen, Y. Li, G. Yu, Z. Zhou and Z. Chen, *J. Chem. Theory Comput.* 2009, **5**, 3088-3095.

53 A. Du, S. C. Smith and G. Lu, *Chem. Phys. Lett.* 2007, **447**, 181-186.

54 J. Qi, X. Qian, L. Qi, Q. Feng, D. Shi and J. Li, *Nano Lett*. 2012, **12**, 1224-1208.

55 W. Chen, Y. Li, G. Yu, C. -Z. Li, S. B. Zhang, Z. Zhou and Z. Chen, *J. Am. Chem. Soc.* 2010, **132**, 1699-1705.

56 Z. Shi, X. Zhao and X. Huang, *J. Mater. Chem. C*, 2013, **1**, 6890-6898.

57 C.-H. Park and S. G. Louie, *Nano Lett*. 2008, **8**, 2200-2203.

58 A. Du, Y. Chen, Z. Zhu, G. Lu and S. C. Smith, *J. Am. Chem. Soc.* 2009, **131**, 1682-1683.

59 J. He, K.Q. Chen, Z. Q. Fan, L. M. Tang and W. P. Hu, *Appl. Phys. Lett.* 2010, **97**, 193305.

60 Z. Yu, M. L. Hu, C. X. Zhang, C. Y. He, L. Z. Sun and J. Zhong, *J. Phys. Chem. C* 2011, **115**, 10836-10841.

61 Y. Liu, X. Wu, Y. Zhao, X. C. Zeng and J. Yang, *J. Phys. Chem. C* 2011, **115**, 9442-9450.

62 Y. Wang, Y. Ding and J. Ni, *J. Phys. Chem. C* 2012, **116**, 5995-6003.

63 R. S. Krsmanović and Z. Šljivančanin, *J. Phys. Chem. C*

2014, **118**, 16104-16112.
64 C. Tang, L. Kou and C. Chen, *Chem. Phys. Lett.* 2012, **523**, 98-103.
65 S. Dutta, A. Manna and S. Pati, *Phys. Rev. Lett.* 2009, **102**, 096601.
66 S. Tang and Z. Cao, *Phys. Chem. Chem. Phys*. 2010, **12**, 2313-2320.
67 B. Huang, M. Liu, N. Su, J. Wu, W. Duan, B. L. Gu and F. Liu, *Phys. Rev. Lett.* 2009, **102**, 166404.
68 Y. Zhang and F. Liu, *Appl. Phys. Lett.* 2011, **99**, 241908.
69 K. Bets and B. Yakobson, *Nano Res*. 2009, **2**, 161-166.
70 P. Lou, *Phys. Status Solidi RRL* 2014, **8**, 187-190.
71 P. Lou, *J. Phys. Chem. C* 2014, **118,** 4475-4482.
72 Z. F. Wang, S. Jin and F. Liu, *Phys. Rev. Lett.* 2013, **111**, 096803.
73 L. V. Keldysh, *Sov. Phys. JETP*, 1965, **20**, 1018-1026.
74 G. Henkelman and H. Jonsson, *J. Chem. Phys*. 2000, **113**, 9978.
75 J. P. Perdew, K. Burke and M. Ernzerhof, *Phys. Rev. Lett.* 1996, **77**, 3865-3868.
76 OpenMX Website. T. Ozaki, H. Kino, J. Yu, M. J. Han, N. Kobayashi, M. Ohfuti, F. Ishii, T. Ohwaki and H. Weng, http://www.openmx-square.org/.
77 T. Ozaki, K. Nishio and H. Kino, *Phys. Rev. B: Condens. Matter* 2010, **81**, 035116.
78 N. Troullier and J. L. Martins, *Phys. Rev. B: Condens. Matter* 1991, **43**, 1993-2006.
79 T. Ozaki, *Phys. Rev. B: Condens. Matter* 2003, **67**, 155108.
80 T. Ozaki and H. Kino, *Phys. Rev. B: Condens. Matter* 2004, **69**, 195113.
81 H. J. Monkhorst, J. D. Pack, *Phys. Rev. B: Condens. Matter* 1976, **13**, 5188-5192.
82 P. Lou, *J. Mater. Chem. C*, 2013, **1**, 2996-3003.
83 P. Lou and J. Y. Lee, *J. Phys. Chem. C* 2010, **114**, 10947-10951.
84 J. D. Gale, *JCS Faraday Trans*. 1997, **93**, 629-637.
85 J. D. Gale and A. L. Rohl, *Mol. Simul.* 2003, **29**, 291-341.
86 D. W. Brenner, *Phys. Rev. B: Condens. Matter* 1990, **42**, 9458-9471.
87 S. L. Mayo, B. D. Olafson and W. A. Goddard, DREIDING: *J. Phys. Chem.* 1990, **94**, 8897-8909.
88 X. Wang, *Phys. Rev. Lett.* 2008, **100**, 156404.
89 S. M. Sze, K. K. Ng, *Physics of Semiconductor Devices*, 3rd ed.; Wiley-Interscience, 2007.
90 G. -H. Ding, C. T. Chan, *J. Phys.: Condens. Matter* 2011, **23**, 205304.
91 Q.Yan, B. Huang, J. Yu, F. Zheng, J. Zang, J. Wu, B. -L. Gu, F. Liu and W. Duan, *Nano Lett*. 2007, **7**, 1469-1473.
92 E. C. Stoner, *Proc. Roy. Soc. A* 1938, **165**, 372-414.
93 J. Nakamura, T. Nitta and A. Natori, *Phys. Rev. B: Condens. Matter* 2005, **72**, 205429.
94 Z. Liu, F. Liu and Y.-S. Wu, *Chinese Phys. B* 2014, **23**, 077308.